Oral Metformin Inhibits Choroidal Neovascularization by Modulating the Gut-Retina Axis

Jason Y. Zhang,[1] Jason Xiao,[1] Bingqing Xie,[2] Hugo Barba,[3] Michael Boachie-Mensah,[1] Rohan N. Shah,[1] Urooba Nadeem,[4] Melanie Spedale,[5] Nicholas Dylla,[6] Huaiying Lin,[6] Ashley M. Sidebottom,[6] Mark D'Souza,[6] Betty Theriault,[5,7] Dinanath Sulakhe,[6] Eugene B. Chang,[2,6] and Dimitra Skondra[3]

[1]Pritzker School of Medicine, University of Chicago, Chicago, Illinois, United States
[2]Department of Medicine, University of Chicago, Chicago, Illinois, United States
[3]Department of Ophthalmology and Visual Science, University of Chicago, Chicago, Illinois, United States
[4]Department of Pathology, University of Chicago, Chicago, Illinois, United States
[5]Animal Resources Center, University of Chicago, University of Chicago, Chicago, Illinois, United States
[6]Duchossois Family Institute, University of Chicago, Chicago, Illinois, United States
[7]Department of Surgery, University of Chicago, Chicago, Illinois, United States

Correspondence: Dimitra Skondra, The University of Chicago, Department of Ophthalmology and Visual Science, 5841 S. Maryland Avenue MC2114, S-426, Chicago, IL 60637-1234, USA; dskondra@bsd.uchicago.edu.

JYZ, JX, BX and HB contributed equally to this study and should be considered co-first authors.

Received: January 19, 2023
Accepted: November 9, 2023
Published: December 18, 2023

Citation: Zhang JY, Xiao J, Xie B, et al. Oral metformin inhibits choroidal neovascularization by modulating the gut-retina axis. *Invest Ophthalmol Vis Sci.* 2023;64(15):21. https://doi.org/10.1167/iovs.64.15.21

Purpose. Emerging data indicate that metformin may prevent the development of age-related macular degeneration (AMD). Whereas the underlying mechanisms of metformin's anti-aging properties remain undetermined, one proposed avenue is the gut microbiome. Using the laser-induced choroidal neovascularization (CNV) model, we investigate the effects of oral metformin on CNV, retinal pigment epithelium (RPE)/choroid transcriptome, and gut microbiota.

Methods. Specific pathogen free (SPF) male mice were treated via daily oral gavage of metformin 300 mg/kg or vehicle. Male mice were selected to minimize sex-specific differences to laser induction and response to metformin. Laser-induced CNV size and macrophage/microglial infiltration were assessed by isolectin and Iba1 immunostaining. High-throughput RNA-seq of the RPE/choroid was performed using Illumina. Fecal pellets were analyzed for gut microbiota composition/pathways with 16S rRNA sequencing/shotgun metagenomics, as well as microbial-derived metabolites, including small-chain fatty acids and bile acids. Investigation was repeated in metformin-treated germ-free (GF) mice and antibiotic-treated/GF mice receiving fecal microbiota transplantation (FMT) from metformin-treated SPF mice.

Results. Metformin treatment reduced CNV size ($P < 0.01$) and decreased Iba1+ macrophage/microglial infiltration ($P < 0.005$). One hundred forty-five differentially expressed genes were identified in the metformin-treated group ($P < 0.05$) with a down-regulation in pro-angiogenic genes *Tie1, Pgf*, and *Gata2*. Furthermore, metformin altered the gut microbiome in favor of *Bifidobacterium* and *Akkermansia*, with a significant increase in fecal levels of butyrate, succinate, and cholic acid. Metformin did not suppress CNV in GF mice but colonization of microbiome-depleted mice with metformin-derived FMT suppressed CNV.

Conclusions. These data suggest that oral metformin suppresses CNV, the hallmark lesion of advanced neovascular AMD, via gut microbiome modulation.

Keywords: age-related macular degeneration (AMD), gut microbiome, angiogenesis, metformin, retinal pigment epithelium (RPE)/choroid

Age-related macular degeneration (AMD) is the leading cause of irreversible blindness in adults over 60 years of age, with its prevalence expected to increase to 22 million in the United States by 2050 and 288 million globally by 2040.[1] Although twice as prevalent as Alzheimer's disease, and similar to invasive cancers combined, there are limited preventative and therapeutic interventions with no cure.[2]

Metformin, the most common anti-diabetic medication, has been found to be protective in several senescence-related conditions, including heart disease and dementia, leading to the Targeting Aging with Metformin (TAME) clinical trial currently under development.[3] Emerging data from our team and other groups suggest that metformin has similar protective effects in AMD, including advanced

neovascular AMD (nAMD), characterized by choroidal neovascularization (CNV).[4–7] Preclinical studies also describe the beneficial effects of metformin in animals and cell lines exposed to stressors that recapitulate AMD pathophysiology.[8] Additionally, a mathematical drug-gene association study from our group predicted metformin as one of the top candidate compounds of value for AMD, particularly nAMD.[9]

However, the underlying mechanism of metformin's beneficial effects remains elusive, as the majority of orally ingested metformin remains confined to the intestinal tract. Recent studies suggest that metformin acts primarily through the reshaping of the gut microbiome, promoting beneficial keystone taxa, and inhibiting harmful counterparts.[10,11] Interestingly, recent studies have explored the effect of diet and environmental stressors on the gut microbiota in nAMD using clinical samples from patients with nAMD and animal models of laser-induced CNV.[12,13] Gut microbial influence in AMD is mainly understood in the context of immune system and angiogenesis modulation by the gut microbiota in the retinal pigment epithelium (RPE) and choroid.[12,14]

Here, we tested the hypothesis that metformin inhibits nAMD features by reshaping the gut microbiome and modulating the gut-retina axis. We elucidate functional interactions between metformin, microbial composition and functions, fecal microbial metabolites, the chorioretinal transcriptome, and CNV. Utilizing specialized germ-free (GF) and colonized gnotobiotic CNV mouse models, we provide evidence that oral metformin's protective effects are mediated mainly by the gut microbiome. The identification of these mechanistic insights into the metformin-nAMD relationship contributes valuable supporting data for the potential repurposing of metformin as a novel therapeutic strategy for AMD via the gut-retina axis.

Materials and Methods

Study Approval

Experiments were performed in accordance with the ARVO Statement for the Use of Animals in Ophthalmic and Vision Research and approved by the Institutional Animal Care and Use Committee of the University of Chicago (protocol #727557).

Animals

Ten-week-old male wild-type C57Bl/6J specific pathogen-free (SPF) mice were purchased from Jackson Laboratories and bred at the Animal Resources Center at the University of Chicago. The mice were kept in sterile, flexible film isolators to strictly control their housing environment. All animals were fed a similar diet and exposed to 12:12 light-dark cycles. Temperature and humidity were maintained per The Guide for the Care and Use of Laboratory Animals.[15]

GF C57Bl/6J mice were housed at the Gnotobiotic Research Animal Facility at the University of Chicago. To maintain sterility, diets (5K67 LabDiet) were autoclaved (121°C for 40 minutes) and weekly fecal pellets were collected for inoculum in bacterial cultures.[16] As a confirmatory test, RT-PCR of the bacterial 16S ribosomal RNA gene was performed on the fecal samples. There were no positive cultures or amplification of 16S bacterial rRNA in any of the GF mice used in this study (Supplementary Fig. S12). A full description of the sterility checks is available in the Supplementary Materials.

Metformin Treatment

SPF mice were treated with either metformin (Sigma, St. Louis, MO, USA) 300 mg/kg or reverse osmosis water (vehicle control) by daily oral gavage. The control and treatment groups were six mice in each group. After laser induction at around 12 weeks of age, the mice were maintained on metformin or vehicle for 1 week until euthanization. In GF groups, metformin solution and vehicle were sterilized via polyethersulfone syringe filtration, and oral gavages were performed within the sterile flexible film isolators.

Microbiome Depletion Via Antibiotic and Antifungal Administration

SPF mice at 9 weeks of age initially received 3-day treatment of 0.01 mg/mL Amphotericin-B, administered via drinking water, followed by 5-day treatment of an antibiotic/antifungal cocktail (0.01 mg/mL amphotericin-B, 1 mg/mL ampicillin, 1 mg/mL neomycin trisulfate salt hydrate, 1 mg/mL metronidazole, and 0.5 mg/mL vancomycin hydrochloride). Two days after discontinuing the cocktail, microbiota transplantation was carried out as described below.

Microbial Isolation and Colonization of Germ-Free and Antibiotic/Antifungal-Treated Mice

To create the donor fecal material, fecal pellets were collected from adult control SPF mice and metformin-treated mice (300 mg/kg for 1 week). The pellets were homogenized in Eppendorf tubes containing freezing solution (sterile saline with 12.5% glycerol), centrifuged at 200 g for 5 minutes, and stored in −80°C until utilized. Recipient mice were 11 weeks old and either GF mice or SPF mice treated with antibiotics/antifungals. Mice were fasted 24 hours prior to fecal microbiota transplantation (FMT). To perform FMT, 200 µL of the fecal slurries were administrated via oral gavage to each mouse. In both the antibiotic/antifungal treated mice and GF mice, mice received FMT with donor fecal material from both control SPF mice and metformin-treated SPF mice. This generated four groups: ABxFMT-CTRL ($n = 12$), ABxFMT-MET ($n = 11$), GFxFMT-CTRL ($n = 6$), and GFxFMT-MET ($n = 6$), respectively. Two rounds of FMT were performed, 1 week apart. At the age of 12 weeks, the mice underwent laser induction, followed by CNV lesion/microglia infiltration analysis and microbiome characterization via 16S rRNA analysis post-week 13.

Laser-Induced Choroidal Neovascularization

We used the laser-induced CNV mouse model, as previously described.[17,18] At age 12 weeks, laser photocoagulation was performed using an argon 532-nm laser (IRIDEX Oculight GLx, Mountain View, CA, USA) attached to a slit-lamp delivery system (Carl Zeiss 30SL-M, Jena, Germany). Laser spots (50-µm spot size, 100-ms duration, and 150-mW power) were applied at 3, 6, 9, and 12 o'clock positions around the optic nerve head. The resultant "bubble" formation indicated rupture of the Bruch's membrane, with the presence of hemorrhage or failure to rupture excluded from

Investigative Ophthalmology & Visual Science

further analysis. Intraperitoneal anesthesia was administered with weight-adjusted dosages of ketamine 100 mg/kg and xylazine 10 mg/kg. For GF studies, sterilization of the laminar flow hood was maintained with chlorine dioxide solution with appropriate gowning, as described in our paper.[18]

Quantification and Immunostaining of CNV Lesions and Iba1+ Macrophages/Microglia

To quantify CNV lesion size and Iba1+ macrophage / microglia infiltration, we performed isolectin-IB4 and Iba1 immunostaining 1-week post-laser induction. Mice were euthanized via a CO_2 chamber and cervical dislocation at age 13 weeks. Eyes were enucleated, fixed in 4% paraformaldehyde at 4°C, and dissected to separate the choroid cup and prepare the sclerochoroidal flatmount.[19,20] Dissected samples were incubated overnight at 4°C in 1:500 Iba1 antirabbit antibody (6A4; FUJIFILM Wako Chemicals, Richmond, VA, USA). After 6 wash cycles (10 minutes/cycle) in TBS-T (0.5% Tween 20), samples were incubated at room temperature for 2 hours in the dark with 1:100 Griffonia Simplicifolia Lectin I (B-1105-2; Vector Laboratories, Newark, CA, USA). Afterward, the tissue was washed for six more cycles in TBS-T and mounted on glass slides with ProLong Gold antifade reagent (ThermoFisher Scientific, Waltham, MA, USA). Flatmounts were visualized using a Leica SP5 confocal microscope (Leica Microsystems, Deerfield, IL, USA) at 200 times magnification. Images were processed in FIJI by performing a maximum-intensity Z-stack projection. Outlines of the isolectin-IB4/Iba1 channels were used to quantify lesion area and Iba1+ macrophages/microglia within the neovascular area, respectively. Data were quantified by two independent masked graders to ensure reliability and validity of measurements.

16S rRNA Sequencing

The V4-V5 region of the 16S rRNA encoding gene was amplified per the Earth Microbiome Project (EMP) 16S Illumina Amplicon Protocol.[21] Sequencing was performed at the High-Throughput Genome Analysis Core (Institute for Genomics and Systems Biology). Sequencing reads were processed by QIIME2[22] pipeline with DADA2 denoising[23] strategy to extract the biome abundance matrix for all samples. A full description of the methodology is presented in the Supplementary Materials.

RNA Sequencing of the Retina and RPE

After enucleation and dissection, the choroid and retina were extracted on ice using a sterile technique. RNAse decontamination solution (RNaseZAP; ThermoFisher Scientific, Waltham, MA, USA) was used to treat all surfaces and equipment. The tissues were then immediately stored in RNAlater (Qiagen, Germantown, MD, USA) separately in RNase free Eppendorf tubes and stored at −80°C until RNA extraction. Extraction was performed using RNeasy (Qiagen), and analyzed using Nanodrop (NanoDrop 2000cc; Thermo Scientific) to determine total RNA concentration before sequencing. RNA quality was assessed using the Bioanalyzer, which confirmed that the samples had an RNA integrity number greater than 9.0.

The RNA was then processed into cDNA and hybridized to the Illumina MouseRef-8 version 2 array and scanned in Illumina HiScan (Illumina, San Diego, CA, USA). FASTQ file management and STAR[24] (version 2.4.2a; Stanford University, Stanford, CA, USA) alignment are described in the Supplementary Materials. The raw gene expression count matrix was generated by featureCounts[25] (version subread-1.4.6-p1) and normalized/analyzed by the R packages edgeR[26] and Limma.[27] Mean fold change in expression level among groups was then calculated. Genes with a fold change of at least 1.5 and adjusted P value < 0.31 were analyzed for choroid. Multiple databases and platforms including Lynx,[28] gene ontology, Kyoto Encyclopedia of Genes and Genomes (KEGG),[29] and STRING[30] were used for annotation, visualization, and integrated discovery.

Shotgun Metagenomic Sequencing

Fecal samples were collected from SPF mice for shotgun metagenomic sequencing. Sample collections occurred before treatment and after sacrifice. Fecal pellets were frozen and stored at −80°C until DNA extraction. Total DNA was extracted using the Qiagen DNeasy PowerSoil Kit (47016; Qiagen). High-throughput sequencing on Illumina NextSeq produced around 7 to 8 million paired-end reads per sample with a read length of 150 base pairs. A full description of the taxonomic classification, assembly, and functional profiling is presented in the Supplementary Materials. Analysis was done in R (version 4.1.2) using function *run_lefse* in package *microbiomeMarker*.[31] Linear discriminant analysis cutoff was set to be greater than 2.5, Kruskal-Wallis P value cutoff at 0.05, and normalization method at counts per million. Transformed count of the significant marker genes was extracted from the matrix and used to calculate the $\log_2$ fold change to the overall mean.

Fecal Metabolomics

Fecal samples were collected at baseline, week 1, and week 2, flash frozen, and stored at −80°C. They were processed for metabolomics analysis at the Duchossois Family Institute Host-Microbe Metabolomics Facility (DFI-HMMF) at the University of Chicago. From fecal material, metabolites were extracted with the addition of extraction solvent (80% methanol spiked with internal standards and stored at −80°C) to pre-weighed fecal samples at a ratio of 100 mg of material per mL of extraction solvent in Bead Ruptor tubes (Fisherbrand; 15-340-154). A full description of the methodology is presented in the Supplementary Materials.

Statistics

Statistical analyses were performed using R (version 4.0.3). Quantitative metabolomic data were analyzed as follows. Data were assessed for normality by visual inspection and Shapiro-Wilks test (rstatix::shapiro_test). It was determined to follow a log-normal distribution. To analyze differences between groups, nonparametric Wilcoxon signed-rank tests (rstatix::wilcox_test) were performed and P values were adjusted, to control for the false discovery rate of multiple comparisons, using the Benjamini-Hochberg method. To determine effect sizes of experimental groups on metabolites, Wilcoxon effects size analysis (rstatix::wilcox_effsize) was performed where magnitudes 0.10 to < 0.30 are considered small effects, 0.30 to < 0.50 are considered moderate effects, and $> = 0.50$ are deemed large effects. Relative-quantitative data were compared to the median values for

each compound. Log_2 fold changes were then calculated as the value divided by the median for that compound. All P values < 0.05 were considered statistically significant.

Results

Oral Metformin Suppresses CNV and Iba1+ Macrophages/Microglial Recruitment Around CNV Lesions

We investigated the ability of oral metformin to inhibit the development of nAMD using the laser-induced CNV mouse model[4] (Fig. 1). Body weight was not affected by treatment (Supplementary Fig. S1A). Metformin suppressed CNV lesion size by 2.1-fold (26,160.4 ± 4834.7 μm^2 vs. 12,572.4 ± 2757.4 μm^2, $P < 0.01$; Fig. 2A). Similar results were obtained when metformin was initiated 2 weeks prior to laser but not when started on the day of laser (Supplementary Figs. S1B–E). Metformin treatment decreased $Iba1^+$ macrophage/microglia infiltration around CNV but not Iba1 signal within the lesion (see Figs. 2A, 2B). To investigate whether these effects were sex-specific, experiments were performed with 12-week-old female mice receiving daily oral metformin 7 days prior and 7 days after laser-induced CNV, which showed significant reduction in average lesion size in the metformin-treated group by 2-fold (29,030.1 μm^2 vs. 14,198.5 μm^2, $P < 0.05$; Supplementary Fig. S2A) and a nonsignificant reduction in Iba1 signal (Supplementary Fig. S2B).

Metformin Modulates Chorioretinal Genes and Pathways Related to Angiogenesis and AMD

We performed high-throughput RNA-sequencing of mouse RPE/choroidal complexes and retinas of lasered mice 1 week after laser treatment, with oral metformin and vehicle controls starting 1 week prior. Detailed lists of differentially expressed genes (DEGs) are available in Supplementary Tables S1A and S1B. In the RPE/choroid, 145 DEGs were identified in the metformin-treated group (139 downregulated and 6 upregulated; Fig. 2C). Enrichment analysis for gene ontology showed that the top 3 biological functions altered are related to angiogenesis, of which 19 genes are affected (Fig. 2E, see Supplementary Tables S1A, S1B). Other pathways influenced by metformin treatment were epithelial-to-mesenchymal differentiation and inflammatory pathways, including chemokine signaling. Notch signaling was altered by metformin treatment in the RPE/choroid (see Fig. 2E, Supplementary Tables S1A, S1B). Upstream regulator analysis revealed transcription factors influenced by metformin treatment, including forkhead box C2 (FOXC2), FOXC1, runt-related transcription factor 3 (RUNX3), and Notch (Fig. 2D, Supplementary Table S1C). Transcription factors and target genes were merged to create a graphical network representation (see Fig. 2D). High-throughput RNA-sequencing of the retina revealed no genes significantly affected by metformin treatment. However, 126 DEGs, of which 53 were upregulated in the metformin group, were identified with a relaxed P value of < 0.01 (Supplementary Fig. S3).

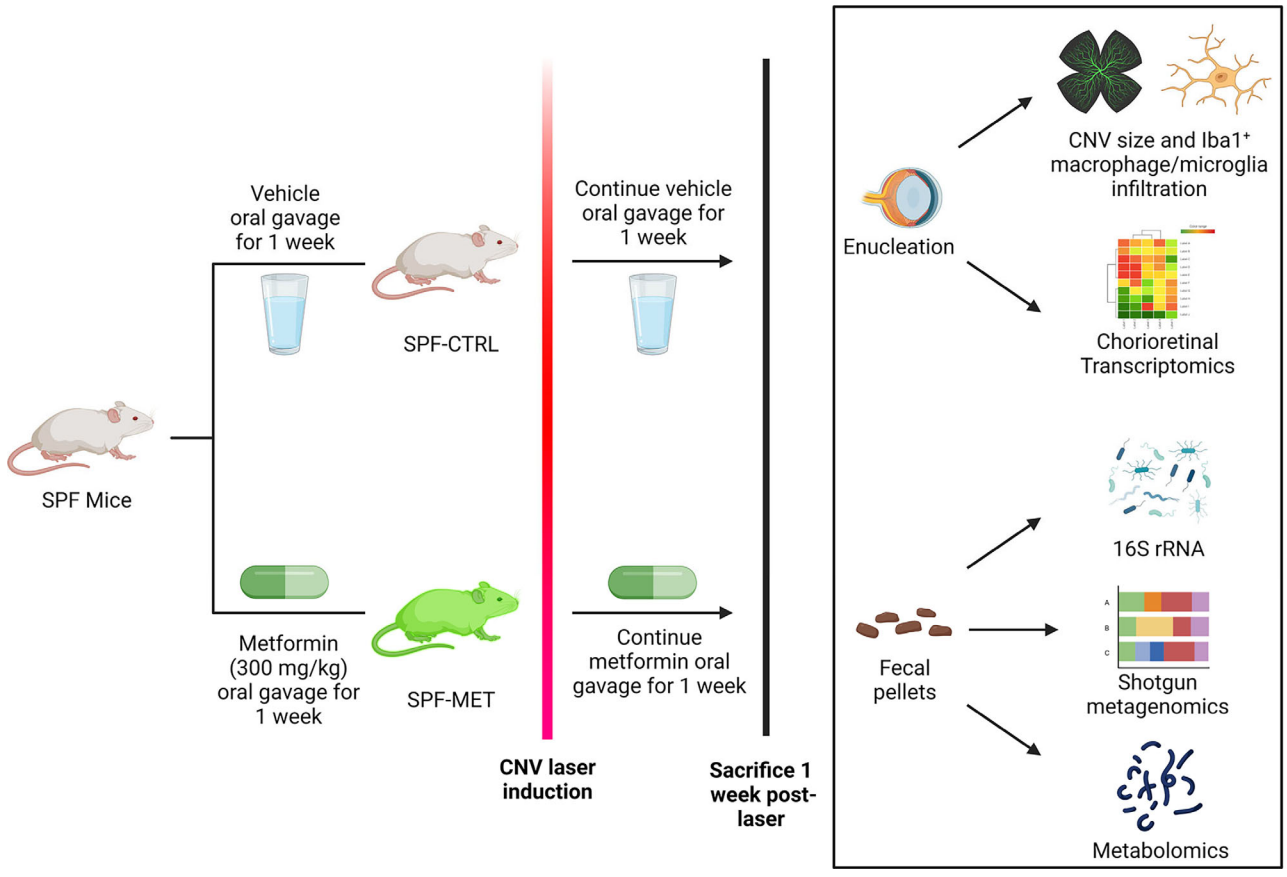

Figure 1. Schematic of SPF-metformin experimental design. Specific pathogen-free (SPF) mice were administered either vehicle (control) or metformin (300 mg/kg) via oral gavage daily for 1-week pre-laser induction and daily for 1-week post-laser induction.

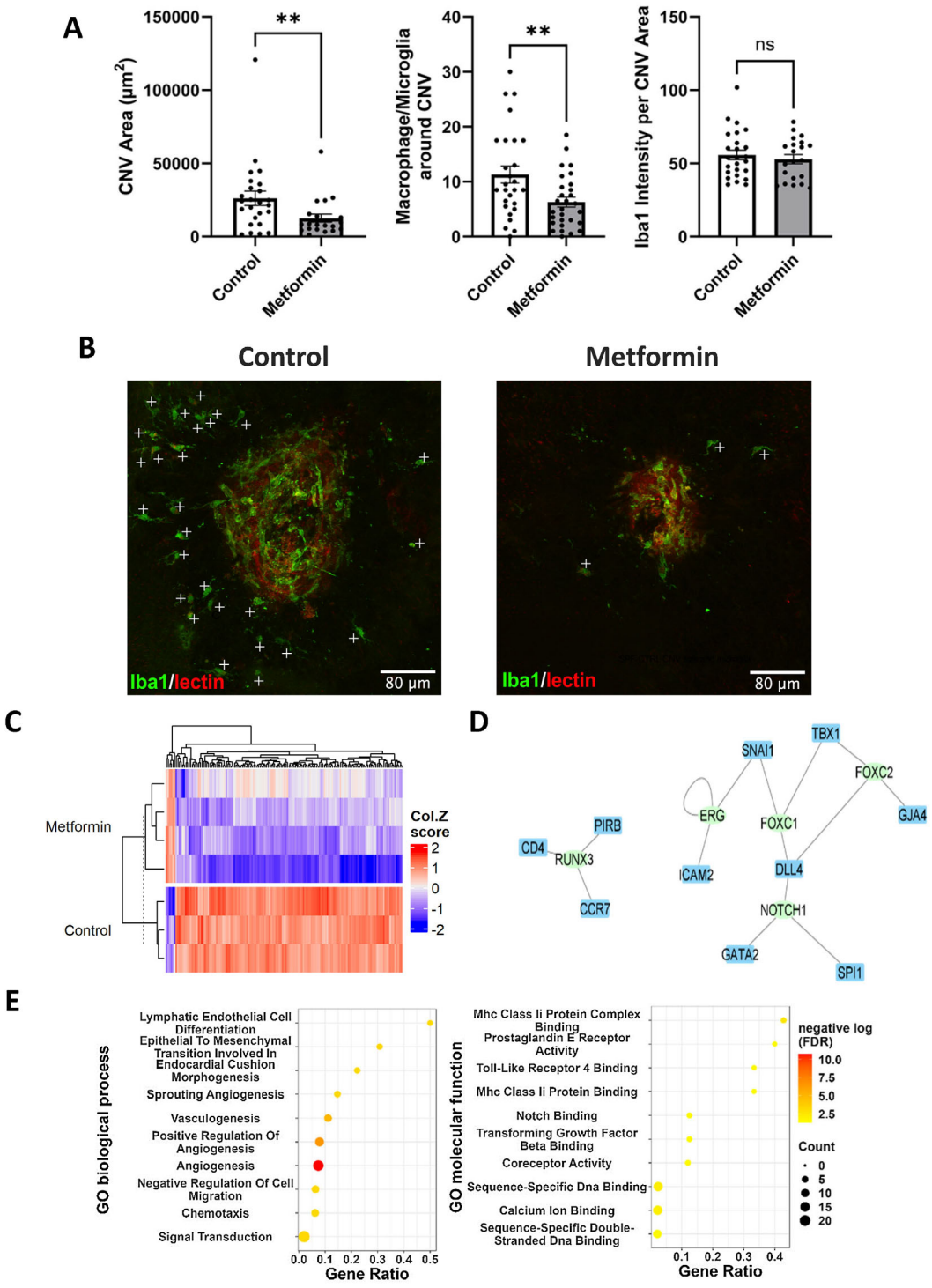

Figure 2. Metformin suppresses CNV size, Iba1+ macrophage/microglial infiltration, and alters RPE/choroid transcriptome. (**A**) Metformin treatment decreases CNV size and Iba1+ macrophage/microglia infiltration around CNV but not Iba1+ macrophage/microglia signal within CNV. $^{**}P < 0.005$; error bars indicate SEM; $n = 6$ per group (SPF-CTRL and SPF-MET). (**B**) Representative RPE/choroid flat-mounts stained with lectin and Iba1 in control vs. metformin-treated mice. +: Iba1+ macrophage/microglia; scale bars: 80 μm. (**C**) Heatmap of the gene expression matrix for differentially expressed genes (DEGs) in the RPE/choroid between control and metformin treated groups (values normalized by sample). One hundred forty-five (145) DEGs (139 downregulated and 6 upregulated) were identified in the metformin-treated group. (**D**) Network of significantly enriched transcription factors and their target genes from RPE/choroid DEG analysis. Significantly altered transcription factors included forkhead box C2 (FOXC2), transcriptional regulator ERG, and Notch. (**E**) Dot plot of top 10 enriched functional terms from RPE/choroid DEG analysis. Top biological processes and molecular functions included angiogenesis regulation, notch binding, and TLR4 binding. Dot size indicates the number of DEGs within the functional category, and dot color reflects adjusted *P* value significance.

Investigative Ophthalmology & Visual Science

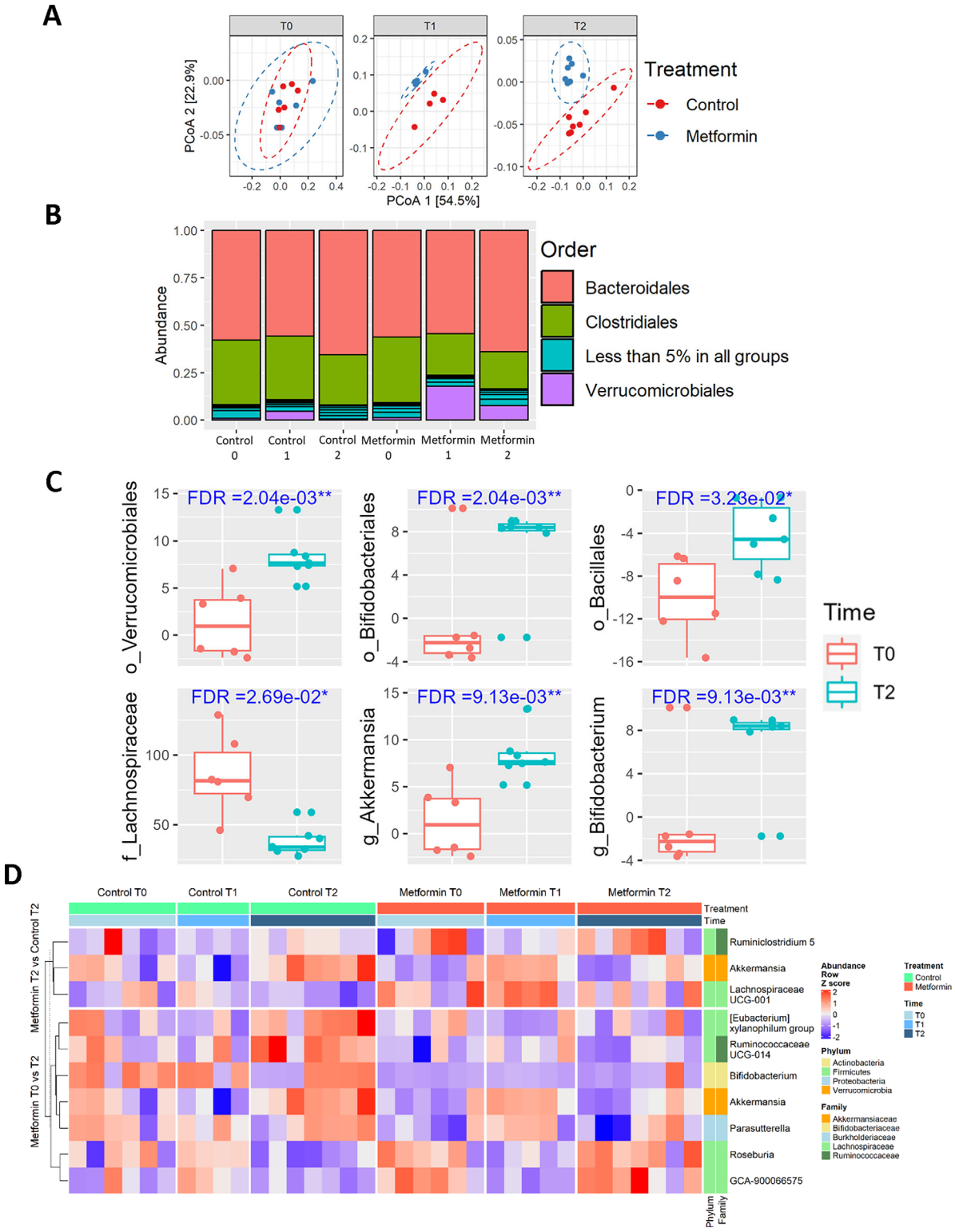

Figure 3. Metformin alters gut microbiome composition. (**A**) Principal coordinate analysis (PCoA) at the OTU level. The two-dimensional PCoA plot shows the beta diversity of the metformin and control samples at three time points (T0, T1, and T2). Metformin-treated mice (*blue ellipse*) gathered together and separately from those in the control group (*red ellipse*) at both week 1 (T1) and week 2 (T2). (**B**) Representative stacked bars of relative bacterial order abundance in gut microbiota of control vs. metformin-treated mice prior to treatment (T0), after 1 week of treatment (T1), and after 2 weeks of treatment (T2); $n = 6$ (control), $n = 6$ (metformin). *Clostridiales* order of *Firmicutes* phylum decreased most significantly in the metformin group by T2, whereas the *Verrucomicrobiales* order increased. (**C**) Boxplots of centered log ratio (CLR) abundances for select differentially detected taxa between metformin T0 and metformin T2 groups, including *Verucomicrobiales* and *Bacillales*. The highlighted FDR value for each subplot is estimated by Limma linear model. (**D**) Heatmap of differentially detected genera (FDR < 0.1) across all samples in two contrast groups: (1) Metformin treated samples at time 0 vs. 2; (2) Control samples versus metformin treated samples at time 2. The abundance values are normalized by sample. Phylum and family level information for genera are shown.

Metformin Alters Gut Microbial Composition and Pathways

The 16S rRNA sequencing was performed on fecal DNA at 3 timepoints: beginning of metformin treatment (T0), after 1 week (T1), and after 2 weeks (T2). Treatment affected both alpha- and beta-diversity (Fig. 3A, Supplementary Figs. S4A, S4B), with oral intake over 2 weeks altering microbial composition. At the order level, *Clostridiales* of *Firmicutes* phylum decreased most significantly in the metformin group by T2, whereas *Verrucomicrobiales* order increased (Fig. 3B). *Clostridia* was the most significantly decreased *Firmicutes* class by metformin at T2 compared to control. Additionally, the metformin T2 group showed an increased abundance of genera *Akkermansia* and *Bifidobacterium* (Fig. 3C). A detailed heatmap illustrating the changes in the abundance of family, phyla, and genera after placebo or metformin treatment is shown in Figure 3D.

Furthermore, we found that 2 weeks of metformin treatment promoted an increased number of positive connections among microbial genera, especially those within *Bacteroidetes*, *Verrucomicrobia*, *Actinobacteria*, and *Firmicutes* phyla (Fig. 4A). A positive correlation was observed between genera from *Verrucomicrobia*, *Bacteroidetes*, and *Actinobacteria* with both the metformin T1 and metformin T2 groups. The genera most associated with increased CNV lesion size were *Marvinbryantia* and *Roseburia*, both members of the *Lachnospiraceae* family (Supplementary Fig. S5). In contrast, the genera *Eubacterium* and *Ruminococcaceae* were protective for CNV.

Twenty-seven (27) functional pathways were significantly altered in mice treated with metformin for 2 weeks compared to controls. Enriched pathway categories included carbohydrate metabolism (pyruvate metabolism, citrate cycle, and butanoate metabolism), energy metabolism (oxidative phosphorylation and carbon fixation), and lipid metabolism. Downregulated pathways included amino acid metabolism, carbohydrate metabolism (starch and sucrose metabolism, pentose phosphate pathway, and C5-branched dibasic acid metabolism), energy metabolism (nitrogen metabolism), and metabolism of cofactors, vitamins, terpenoids, polyketides, and nucleotides (Fig. 4C).

Microbiome-Transcriptome Networks in the RPE/Choroid Show Negative Associations Between *Akkermansia* and Choroidal Neovascularization

We analogously constructed association networks using ENSEMBLE version 3.0[32] with 16S microbial and RPE/choroid transcriptome data (Fig. 4B). In this network, the mean number of genes associated with each class was 20 and each genus was 16. *Akkermansia* was the clear hub genus, associated with 26 genes. Genes *Ccl11* and *Rspo3*, which correlated with *Akkermansia*, participate in DEG-enriched Gene Ontology (GO) term angiogenesis (false discover rate [FDR] = 1.66E-11).

Microbial-Derived Short-Chain Fatty Acids and Bile Acid Metabolites are Affected by Metformin

Targeted quantitative and qualitative metabolomic analysis of fecal short-chain fatty acids (SCFAs) and bile acid metabolites were performed at the T0, T1, and T2 time points. Metformin for 2 weeks significantly increased fecal concentrations of butyrate and propionate (Figs. 5A, 5B). A heatmap was plotted using $\log_2$ fold changes relative to the compound's median value (Supplementary Fig. S8).

Fecal contents were also quantitatively analyzed for an array of primary, secondary, and tertiary bile acids. In the metformin T2 group, the fecal levels of cholic, deoxycholic, and isodeoxycholic acids were significantly elevated compared to metformin T0 (Figs. 5C–E). In contrast, metformin treatment decreased fecal levels of lithocholic, alloisolithocholic, and 3-oxolithocholic acids (Figs. 5F–H). A heatmap was constructed using the relative quantitation of fecal levels of 39 bile acids (Supplementary Fig. S10). In fecal samples, metformin treatment elevated three primary bile acids: cholic acid, chenodeoxycholic acid, and muricholic acid. Elevated secondary bile acids included deoxycholic acid and its derivatives: isodeoxycholic acid, taurodeoxycholic acid (TDCA), tauroursodeoxycholic acid (TUDCA), and ursodeoxycholic acid (UDCA). Derivatives of chenodeoxycholic acid and muricholic acid were also increased in the metformin-treated cohort, particularly by week 2 (Supplementary Fig. S11).

Metformin's Inhibitory Effects on CNV are Mediated by the Gut Microbiome

To assess whether metformin's ability to inhibit CNV was dependent on the gut microbiome, we investigated whether metformin treatment remained protective in the absence of the microbiome. The 11-week-old male GF mice were treated with either daily metformin or vehicle starting 1 week prior to laser and maintained for 1 week post-laser, similar to the SPF experiments (Fig. 6A). Metformin treatment did not suppress CNV or Iba1+ macrophages/microglia infiltration in the absence of the microbiome in GF mice (Figs. 7A, 7B).

Meanwhile, FMT was performed on antibiotic/antifungal-treated and GF mice using feces from 2-week metformin-treated and vehicle-treated SPF donor mice (Figs. 6B, 6C). In the antimicrobial/antifungal groups, mice transplanted with fecal material from metformin-treated SPF mice exhibited a 2.1-fold decrease in CNV size and decreased Iba1+ macrophages/microglia around CNV (Figs. 7C, 7D). In GF-FMT mice, results were largely congruent; GF mice receiving FMT from metformin-treated mice exhibited a 2-fold decrease in CNV size along with significant decreases in Iba1+ macrophages/microglia both in and around the lesion (Figs. 7E, 7F). Post-FMT 16S sequencing of fecal pellets in mice that received FMT from donors treated with metformin confirmed successful transplantation and showed changes in microbial profiles compared to controls (Figs. 8, 9). Antibiotic-treated mice receiving FMT showed moderate separation on principal coordinates analysis (PCoA; see Fig. 8A), with $p(F) < 0.001$ (Supplementary Fig. S13). Specific compositional changes included a significant decrease in order *Clostridiales* alongside multiple genera under *Clostridia*, including *Murimonas*, *Papillibacter*, and *Ruminococcus*. Genus *Clostridium_XVIII* of class *Erysipelotrichia* also decreased (see Figs. 8B–D). GF mice receiving FMT showed less separation on PCoA compared to antibiotic-treated mice (see Fig. 9A), with $p(F) = 0.060$ (Supplementary Fig. S14). In the GF group, metformin FMT resulted in a decrease in genera *Butyrivibrio*, *Murimonas*, and *Anaerobacterium* – all of which belong to class *Clostridia*. Other changes included a decrease in family *Enterococcaceae* of class *Bacilli* and phylum *Firmicutes*

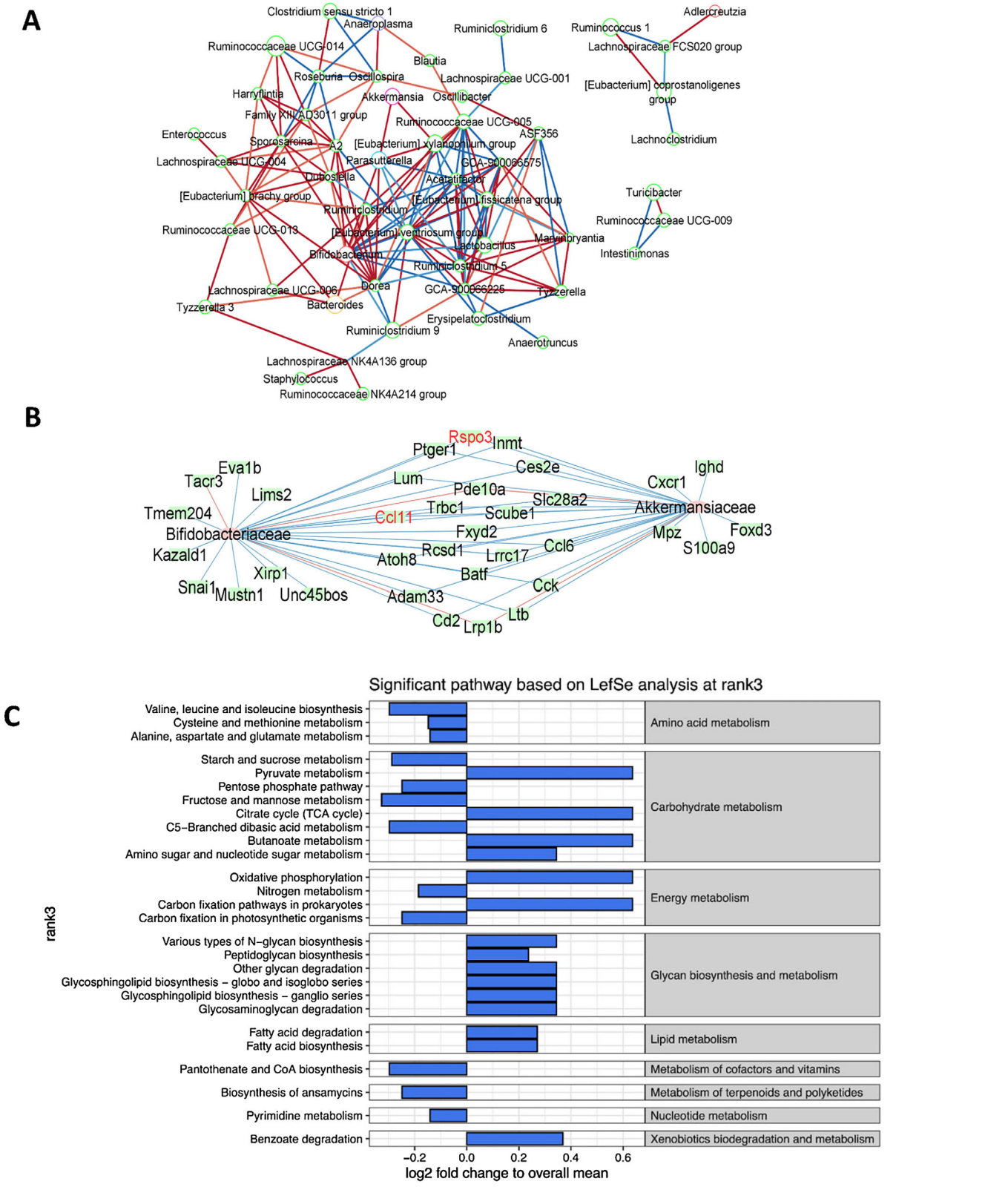

Figure 4. Metformin-associated alterations in microbiome composition are tied to transcriptomic and functional changes. (**A**) Network illustrating significant ($P < 0.05$) microbiome genera co-abundances within the metformin treated group as determined by Pearson's correlation. Metformin treatment for 2 weeks promoted an increased number of positive connections among microbial genera, especially those within *Bacteroidetes*, *Verrucomicrobia*, *Actinobacteria*, and *Firmicutes* phyla. Network edges indicate positive (*red*) and negative (*blue*) correlations. Network nodes are colored by phylum origin. (**B**) Network illustrating significant ($P < 0.05$) Pearson's correlation between RPE/choroid RNA-seq gene expression and 16S microbiome genus level abundance at T2 in matched mice. Genes *Ccl11* and *Rspo3* (*highlighted in red*) are involved in angiogenesis and correlate with hub genus *Akkermansia*. (**C**) LEfSe rank plot of differentially abundant pathways in the gut microbiomes of mice treated with metformin for 2 weeks (metformin T2, $n = 4$) versus the same mice prior to treatment (metformin T0, $n = 4$) and control mice after 2 weeks (control T2, $n = 4$). Twenty-seven (27) abundant pathways were significantly altered, including enrichment in pyruvate and lipid metabolism and downregulation in CoA biosynthesis and amino acid metabolism.

Investigative Ophthalmology & Visual Science

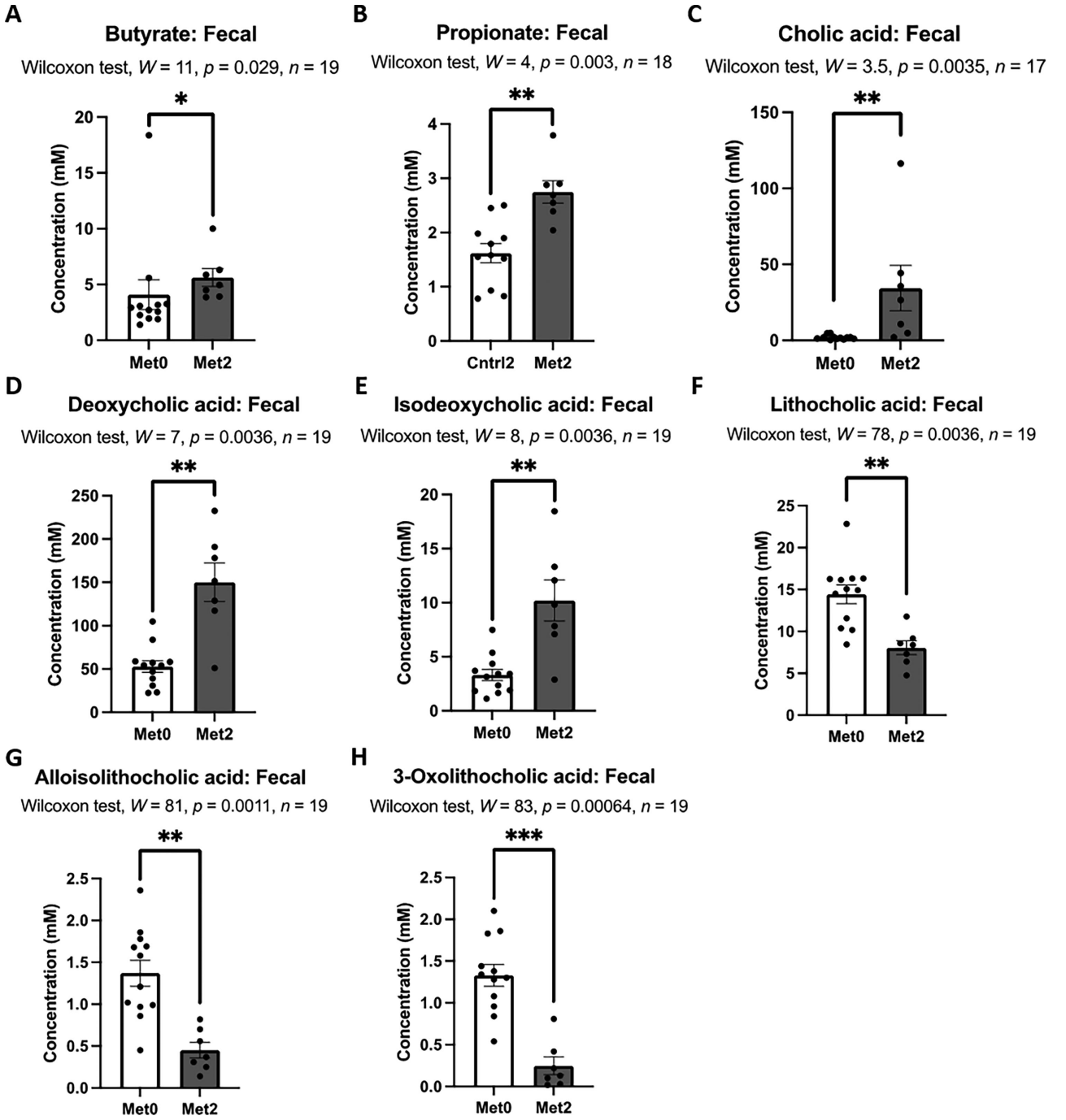

Figure 5. Metformin alters fecal levels of short-chain fatty acids, bile acids, and other metabolites. Levels of short-chain fatty acids (SCFAs), branched-chain fatty acids, amino acids, bile acids, and phenolic metabolites were measured in fecal samples of mice at baseline (Met0), after 1 week of metformin treatment (Met1), after 2 weeks of metformin treatment (Met2), and for age-matched controls of Met2 (Cntrl2). (**A**) Elevated levels of fecal butyrate were detected in Met2 compared to Met0. (**B**) Fecal propionate was increased in Met2 compared to Cntrl2. (**C–E**) Quantitative boxplots comparing Met0 to Met2 revealed elevations of fecal (**C**) cholic acid, (**D**) deoxycholic acid, and (**E**) isodeoxycholic acid in Met2 compared to Met0. (**F–H**) In contrast, metformin treatment decreased fecal levels of (**F**) lithocholic acid, (**G**) alloisolithocholic acid, and (**H**) 3-oxo-lithocholic acid. Statistical testing was performed using the Wilcoxon signed-rank tests, with *P* values adjusted by false discovery rate using the Benjamini-Hochberg method.

(see Figs. 9B–D). A full list of all differential abundance changes is included in Supplementary File S1. Targeted QT-PCR of the genes *Dll4*, *C5ar1*, *Ccl11*, *Pgf*, and *Tie1* did not reveal statistically significant differences between GF control and metformin-treated mice (Supplementary Table S2).

Discussion

The potential protective effects of metformin on AMD have attracted considerable interest in recent years. In this study, we demonstrate that a short course of oral metformin inhibits CNV in mice and alters angiogenesis- and

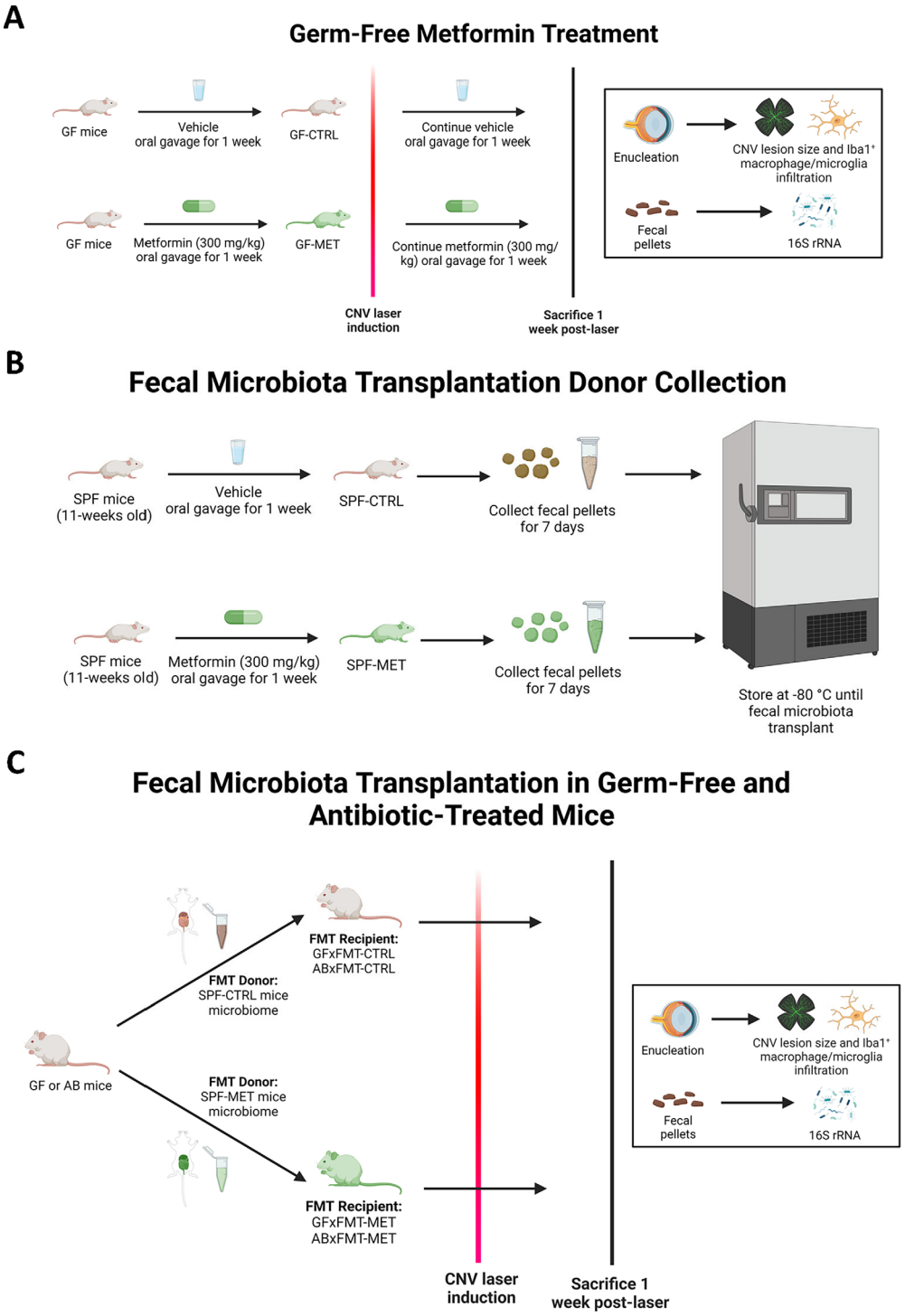

Figure 6. Schematic of GF-metformin and fecal microbiota transplantation (FMT) experiments. (**A**) Germ-free (GF) mice were given metformin or vehicle via oral gavage 1 week prior to laser induction. (**B**) Fecal microbiota transplantation (FMT) was performed using feces collected from donors treated with either metformin or vehicle for 2 weeks. (**C**) GF and antibiotic (AB)-treated mice received FMT for 1 week followed by CNV laser induction and euthanization 1-week post-laser.

AMD-related chorioretinal pathways via modulation of gut microbiota and microbiota-derived metabolites. These findings are in line with emerging data of a link between the gut microbiome and CNV pathogenesis and provide exciting insight that modulating the gut microbiome with interventions, such as metformin, can reduce CNV features.

Effects of short-term metformin intake on gut microbiota composition have not been investigated to date. Interestingly, several human and animal studies have linked the gut microbiome to metformin's mechanism of action, citing its ability to maintain the gut barrier and promote butyrate-producing bacteria (e.g. *Akkermansia*), as seen

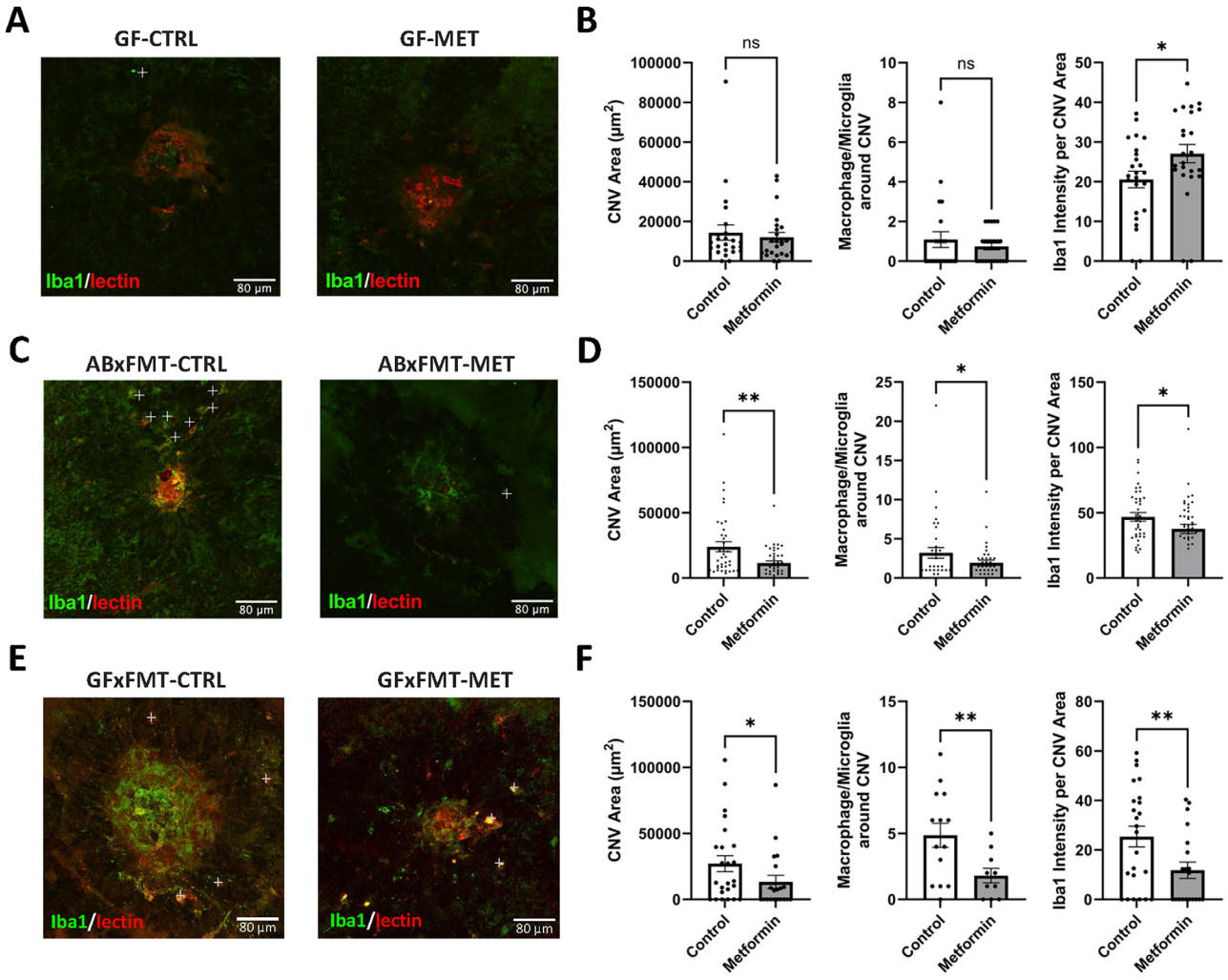

Figure 7. Metformin's inhibitory effects on CNV are mediated by the gut microbiome. (**A, B**) GF mice treated with metformin showed no difference in CNV and Iba1+ macrophages/microglia infiltration compared to vehicle-treated counterparts. However, FMT from metformin-treated SPF mice (FMT-MET) reduced CNV size and Iba1+ macrophages/microglia infiltration in (**C, D**) antibiotic-treated and (**E, F**) GF mice.

in our study. Notably, this was shown to improve retinal neuroprotection.[33,34] *Bifidobacterium*, a known probiotic that improves gut immunity and barrier function,[35,36] is diminished in patients with severe AMD, indicating that metformin may be protective through its increased abundance.[14] Furthermore, multiple species of *Akkermansia* and *Bifidobacterium* are decreased in other ocular inflammatory diseases, such as uveitis.[37] *Clostridia's* relative abundance was most influenced by metformin intake and is associated with AMD features in patients and animal models.[38] In our study, however, not all subgroups of *Clostridia* were decreased by metformin intake. Interestingly, families of *Clostridia* decreased by metformin treatment have been associated with worsening of retinal diseases. Specifically, Roseburia is more abundant in patients with proliferative diabetic retinopathy and retinal artery occlusion.[39,40] The distinct influence of oral metformin intake on other families of *Clostridia* is also uncovered by the co-occurrence network, which is not readily appreciated by relative abundance analyses. For instance, *Oscillibacter* and *Oscillospira*, also associated with AMD, are decreased by metformin treatment.[41] Similarly, patients with nAMD have shown increased microbial functional pathways including L-alanine fermentation, glutamate degradation, and arginine biosynthesis.[41] Our results indicate that metformin treatment may reverse these characteristic profiles – a key change since amino acids and polyunsaturated fatty acids play crucial roles in retinal function.[42–49] Thus, metformin alters the microbial metagenome in a potentially beneficial manner, leading to modulated functional pathways that are integral to AMD pathogenesis.[42,47,50]

Meanwhile, metformin's effects on the RPE/choroidal transcriptome demonstrate that most of the metformin-regulated genes encoded angiogenesis-related functions, including downregulation of pro-angiogenic genes *Tie1, Pgf*, and *Gata2*. *Tie1* is a major player in pathologic angiogenesis pathways and a suggested target of therapeutic intervention in retinal vascular diseases including nAMD.[51–53] Besides the association of *Pgf* and *Gata2* with VEGF pathways, *Pgf* has been identified as a susceptibility gene in specific nAMD populations.[54–56] This transcriptomic effect extends to inflammatory and immune processes in the retina as well, potentially regulating CNV progression. Meanwhile, it is well-documented that the complement system plays

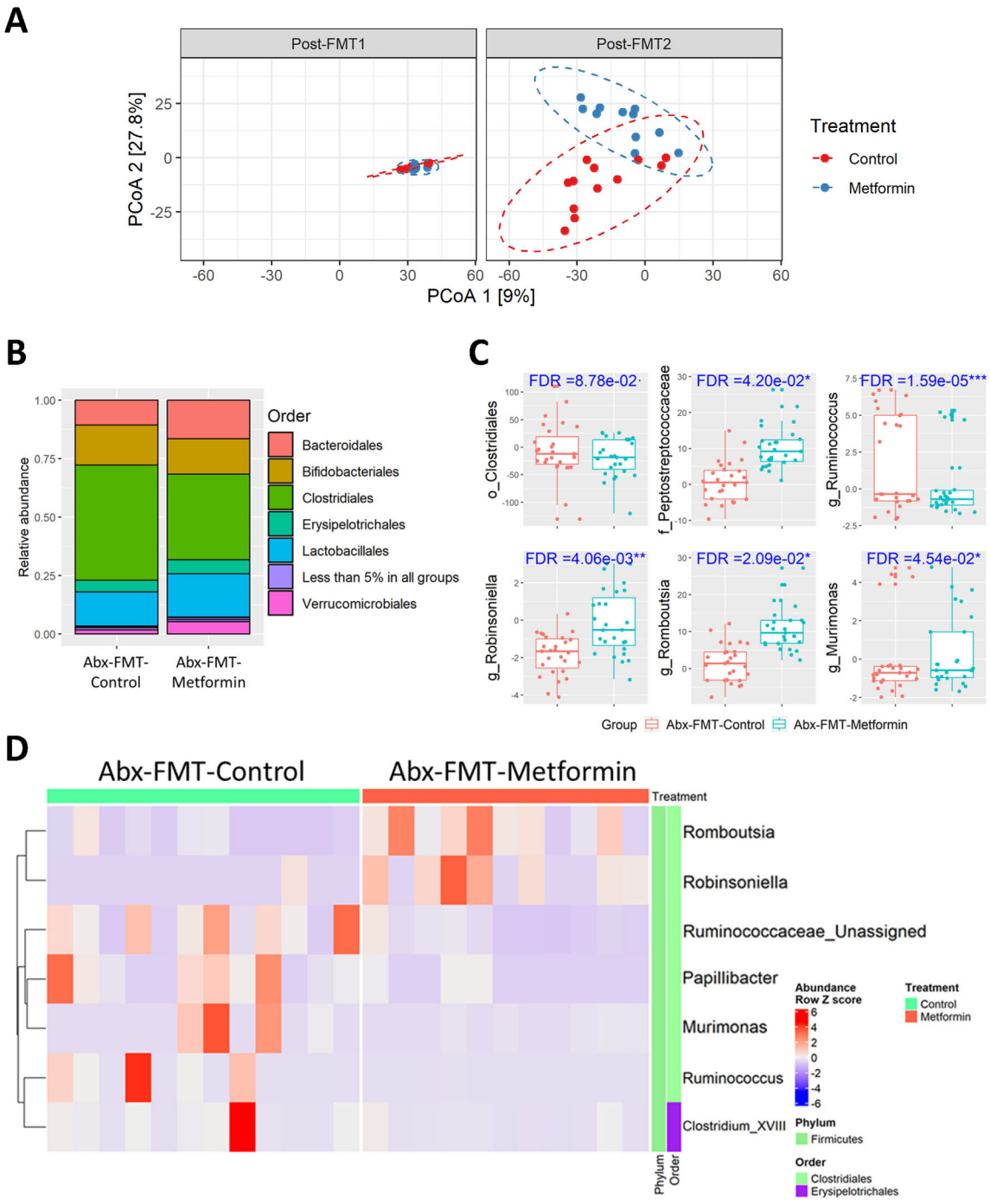

Figure 8. FMT from metformin-treated SPF mice changes microbiome composition in antibiotic-depleted mice (Abx). (**A**) Principal coordinate analysis (PCoA) at the OTU level for antibiotic-treated mice receiving FMT shows moderate separation after two treatments (post-FMT2, $n = 11$). (**B**) Representative stacked bars of relative bacterial order abundance in gut microbiota show a decrease in *Clostridiales* and upward trend in *Bacteroidales* and *Verrucomicrobiales* with metformin FMT. (**C**) Boxplots of CLR abundances for select differentially detected taxa. FMT from metformin-treated SPF mice resulted in a significant decrease in order *Clostridiales* (logFC = −0.95) alongside multiple genera under *Clostridia*, including *Murimonas* (logFC = −2.76), *Papillibacter* (logFC = −2.08), and *Ruminococcus* (logFC = −6.03). Genus *Clostridium_XVIII* of class *Erysipelotrichia* also decreased (logFC = −2.17). (**D**) Heatmap of differentially detected microbiome genera (FDR < 0.1). Abundance values are normalized by sample. Phylum and order level information for genera are shown.

an integral role in the pathogenesis of AMD and CNV formation.[57] Thus, the metformin group's downregulation of complement component C5AR1 may function in a protective role when paired with C3 inhibition. The downregulation of cytokine CCL11, a ligand for CCR3, further supports the protective role of metformin as evidenced by CCR3's expression in AMD-induced CNV lesions.[58] When compared to results from prior literature, such as Xu et al., our results did not show significant change in specific genes related to mitochondrial function, including *Parp14*, *Gadd45b*, and *Coxii*.[59]

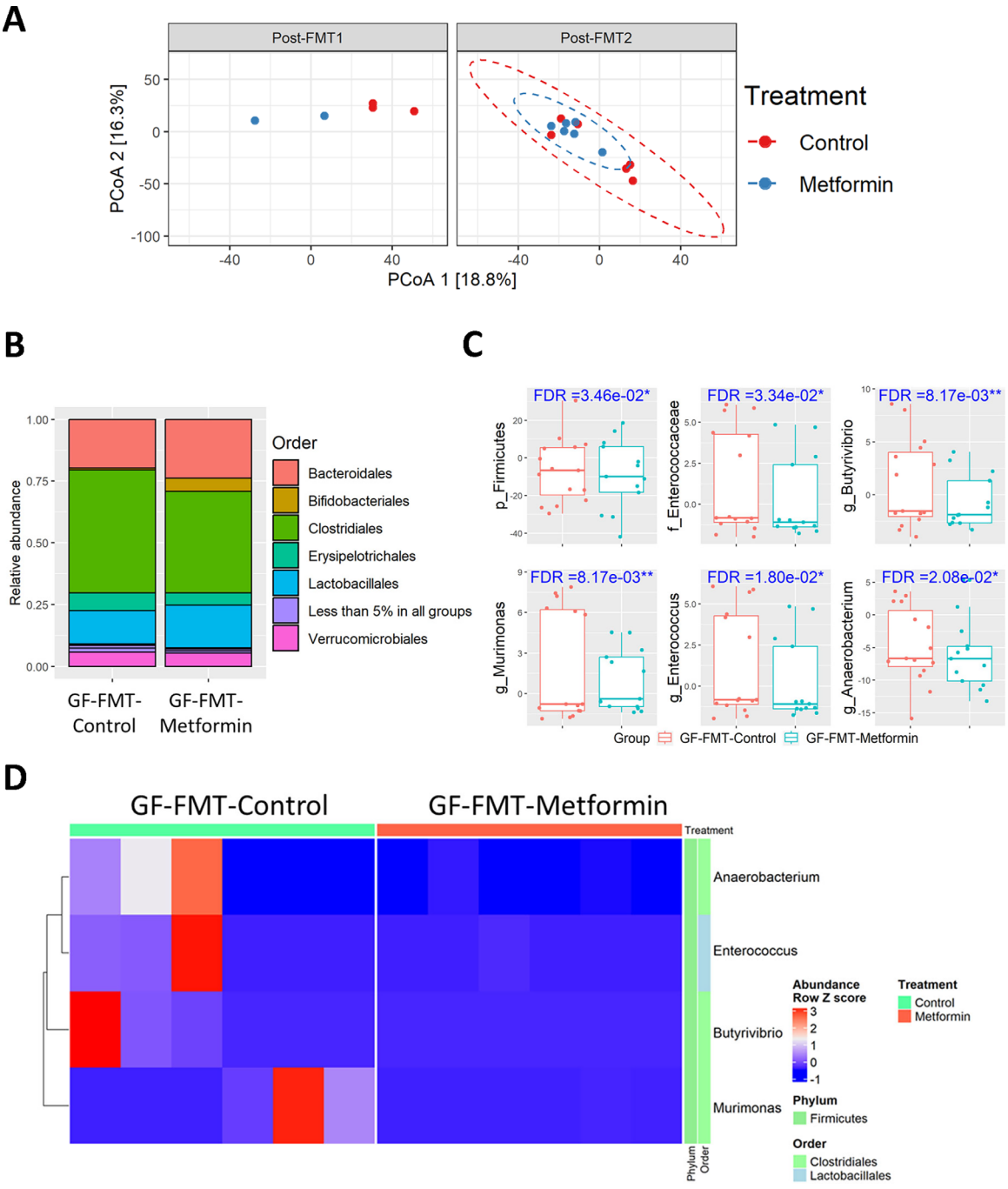

Figure 9. FMT from metformin-treated SPF mice changes microbiome composition in germ-free (GF) mice. (**A**) Principal coordinate analysis (PCoA) at the OTU level for GF mice receiving FMT shows less separation after two treatments (post-FMT2, $n = 6$) compared to antibiotic-treated mice. (**B**) Representative stacked bars of relative bacterial order abundance in gut microbiota show a decrease in *Clostridiales* and upward trend in *Bacteroidales*, *Bifidobacteriales*, and *Lactobacillales* with metformin FMT. (**C**) Boxplots of CLR abundances for select differentially detected taxa. FMT from metformin-treated SPF mice resulted in a significant decrease in genera *Butyrivibrio* (logFC = −5.82), *Murimonas* (logFC = −6.58), and *Anaerobacterium* (logFC = −5.53) from class *Clostridia*. Other changes included a decrease in family *Enterococcaceae* (logFC = −4.96) of class *Bacilli* and phylum *Firmicutes* (logFC = −0.86). (**D**) Heatmap of differentially detected microbiome genera (FDR < 0.1). Abundance values are normalized by sample. Phylum and order level information for genera are shown.

However, our transcriptomic data stems from oral metformin delivery compared to subcutaneous delivery with Xu et al. This suggests that metformin may differentially impact transcriptomic expression in the RPE/choroid depending on its systemic availability with subcutaneous delivery or recruitment of the microbiome with oral delivery. Additionally, Xu et al. specifically analyzed retinal tissue, whereas here we focused on the RPE/choroid, suggesting spatial transcriptomic differences may exist in response to metformin treatment.

Although it is unclear how metformin drives these changes in peripheral tissues, there are a number of possibil-

ities. The absent protective effects of metformin in GF mice, and reconstituted protection with microbial transplantation from donors treated with metformin, imply a direct role for the microbiome in mediating metformin's actions. One explanation may lie with metformin-mediated alterations in the metabolome. With metformin treatment, we identified significant elevations in fecal SCFAs, butyrate and propionate, which is consistent with human metformin studies demonstrating similar shifts in microbial composition.[60–62] SCFAs regulate intestinal epithelial integrity and host immunity, with studies suggesting that regulation of retina-specific T-cells may rely on gut microbiota interactions.[63] In addition to regulating immune and inflammatory responses, butyrate has also been shown to diminish CNV lesion size, with supporting in vitro evidence of reduced VEGFA and VEGFR2 signaling.[64,65] SCFAs may also contribute to RPE-choroid transcriptional changes. For example, SCFAs can downregulate complement system expression, including C5AR1, which was found downregulated in the RPE-choroid.[66] Therefore, metformin's protective effects on CNV lesion size and macrophage/microglia recruitment may partly result from increased levels of butyrate and propionate, which can modulate angiogenesis, immunity, and/or transcriptional pathways in the eyes.

In addition to SCFAs, bile acids were also altered by metformin, including increased relative abundances of microbiota-associated metabolites UDCA and TUDCA. These molecules' neuroprotective effects have been examined in various neurologic diseases and may extend to retinal pathology.[67] For example, UDCA has been shown to attenuate blood-retinal barrier breakdown and inflammation by modulating expression of tight junction proteins, VEGF, NFκB, and iNOS.[68] In nAMD mouse studies, oral UDCA significantly reduced laser-induced CNV lesion size and decreased VEGF protein expression.[69] These findings are corroborated in nAMD rat models, where TUDCA or UDCA treatment before and after laser-induced CNV successfully reduced lesion size.[70] Altogether, the increased relative abundance of TUDCA and UDCA following metformin treatment may partly explain the microbiome-dependent protection of oral metformin on CNV lesion size and macrophage/microglia recruitment.

Our study has several limitations. One cannot be sure if the protective effects of metformin against CNV are from direct effects of systemically absorbed metformin, as the quantity of drug present in ocular tissue was not determined. Nevertheless, our GF and FMT experiments demonstrate that metformin's effects are at least partially mediated by gut-retina axis modulation. Second, the laser-induced CNV model does not completely represent nAMD, as the human retina's anatomy and physiology differ from animal models. Similarly, these changes in the mouse microbiome may not translate to changes in the human microbiome. Studies that assess functional changes and incorporate proteomics within the RPE/choroid are needed. Furthermore, laser-induced CNV lesions only represent a small portion of chorioretinal tissue analyzed for transcriptomics, which may have diluted the number and fold-changes of the affected DEGs. Finally, it is important to acknowledge that our study included only male mice. Previous studies have shown increased susceptibility to CNV among female mice, postulated to be tied to expression levels of estrogen and its pro-angiogenic effects.[71–73] Additionally, cellular and molecular response to metformin varies by sex across multiple tissue types, including neurologic tissue.[74,75] Levels of metformin achieved in plasma and the brain also depend on sex.[76] Furthermore, it has been shown that metformin alters gut microbiome composition and metabolic markers differently by sex.[77,78] Given this, further study is needed to elucidate sex-specific differences in CNV progression and rescue in the context of metformin use.

Our report provides an initial description of the inhibitory effects of oral metformin on CNV, the hallmark lesion in nAMD, by modulating microbial composition, fecal metabolomics, and RPE/choroid transcriptomics. This study provides new insight into a potential novel treatment strategy for AMD by harnessing metformin's protective effects on the gut-retina axis. Future studies are needed to further delineate the underlying mechanisms of how metformin induces changes to specific microbial populations and interacts with nAMD-related pathogenesis.

Acknowledgments

Supported by Genentech AMD Research Fellowship "Common antidiabetic drug metformin prevents AMD by reshaping the gut microbiome" (D. Skondra), Institute for Translational Medicine (D. Skondra), BrightFocus Foundation "Role of high fat diet and gut microbiome in macular degeneration" (D. Skondra, M2018042), NIDDK P30 (E.B.C., DK42086), The University of Chicago Women's Board (D. Skondra), FORE-I Foundation (D. Skondra), and the Illinois Society for the Prevention of Blindness (D. Skondra, FP067271-01-PR).

Author Contributions: D. Skondra designed research. H.B., M.B.M., R.N.S., M.S., and B.T. performed experiments. J.Y.Z., J.X., B.X., M.S., D. Skondra, D. Sulakhe, H.B., M.B.M., R.N.S., U.N., N.D., A.S., and H.L. collected and analyzed data.; J.Y.Z., J.X., B.X., U.N., M.B.M., D. Skondra, E.B.C., A.M.S., B.T., and M.B.M. prepared and reviewed the manuscript.

Disclosure: **J.Y. Zhang**, None; **J. Xiao**, None; **B. Xie**, None; **H. Barba**, None; **M. Boachie-Mensah**, None; **R.N. Shah**, None; **U. Nadeem**, None; **M. Spedale**, None; **N. Dylla**, None; **H. Lin**, None; **A.M. Sidebottom**, None; **M. D'Souza**, None; **B. Theriault**, None; **D. Sulakhe**, None; **E.B. Chang**, None; **D. Skondra**, None

References

1. Wong WL, Su X, Li X, et al. Global prevalence of age-related macular degeneration and disease burden projection for 2020 and 2040: a systematic review and meta-analysis. *Lancet Glob Health*. 2014;2(2):e106–e116.
2. Pennington KL, DeAngelis MM. Epidemiology of age-related macular degeneration (AMD): associations with cardiovascular disease phenotypes and lipid factors. *Eye Vision (London, England)*. 2016;3:34.
3. Barzilai N, Crandall JP, Kritchevsky SB, Espeland MA. Metformin as a tool to target aging. *Cell Metab*. 2016;23(6):1060–1065.
4. Blitzer AL, Ham SA, Colby KA, Skondra D. Association of metformin use with age-related macular degeneration: a case-control study. *JAMA Ophthalmol*. Published online January 21, 2021, doi:10.1001/jamaophthalmol.2020.6331.
5. Romdhoniyyah DF, Harding SP, Cheyne CP, Beare NAV. Metformin: a potential role in age-related macular degeneration: a systematic review and meta-analysis. *Ophthalmol Ther*. 2021;10(2):245–260.
6. Brown EE, Ball JD, Chen Z, Khurshid GS, Prosperi M, Ash JD. The common antidiabetic drug metformin reduces odds of developing age-related macular degeneration. *Invest Ophthalmol Vis Sci*. 2019;60(5):1470–1477.

7. Stewart JM, Lamy R, Wu F, Keenan JD. Relationship between oral metformin use and age-related macular degeneration. *Ophthalmol Retina*. 2020;4(11):1118–1119.
8. Qu S, Zhang C, Liu D, et al. Metformin protects ARPE-19 cells from glyoxal-induced oxidative stress. *Oxid Med Cell Longev*. 2020;2020:1740943.
9. Xie E, Nadeem U, Xie B, et al. Drug-gene association analysis to identify novel AMD therapeutics. *Invest Ophthalmol Vis Sci*. 2021;62(8):217.
10. Prattichizzo F, Giuliani A, Mensà E, et al. Pleiotropic effects of metformin: shaping the microbiome to manage type 2 diabetes and postpone ageing. *Ageing Res Rev*. 2018;48:87–98.
11. Torres W, Nava M, Galbán N, et al. Anti-aging effect of metformin: a molecular and therapeutical perspective. *Curr Pharm Des*. 2020;26(35):4496–4508.
12. Andriessen EM, Wilson AM, Mawambo G, et al. Gut microbiota influences pathological angiogenesis in obesity-driven choroidal neovascularization. *EMBO Mol Med*. 2016;8(12):1366–1379.
13. Rowan S, Taylor A. Gut microbiota modify risk for dietary glycemia-induced age-related macular degeneration. *Gut Microbes*. 2018;9(5):452–457.
14. Zysset-Burri DC, Keller I, Berger LE, et al. Associations of the intestinal microbiome with the complement system in neovascular age-related macular degeneration. *NPJ Genom Med*. 2020;5(1):1–11.
15. National Research Council US) Committee for the Update of the Guide for The Care and Use of Laboratory Animals. *Guide for the Care and Use of Laboratory Animals*. Washington, DC: National Academies Press; 2011, doi:10.17226/12910.
16. Theriault B, Wang Y, Chen L, Vest A, Bartman C, Alegre ML. Long-term maintenance of sterility following skin transplantation in germ-free mice. *Transplant Direct*. 2015;1(8):e28.
17. Shah RS, Soetikno BT, Lajko M, Fawzi Amani AA. A mouse model for laser-induced choroidal neovascularization. *J Vis Exp*. 2015;2015(106):e53502.
18. Movahedan A, Barba H, Spedale M, et al. Gnotobiotic operations and assembly for development of germ-free animal model of laser-induced choroidal neovascularization. *Transl Vis Sci Technol*. 2021;10(9):14.
19. Claybon A, Bishop AJR. Dissection of a mouse eye for a whole mount of the retinal pigment epithelium. *J Vis Exp*. 2011;48:2563.
20. Ivanova E, Toychiev AH, Yee CW, Sagdullaev BT. Optimized protocol for retinal wholemount preparation for imaging and immunohistochemistry. *J Vis Exp*. 2013;82:e51018.
21. Protocols and Standards : earthmicrobiome. Accessed July 28, 2022. Available at: https://earthmicrobiome.org/protocols-and-standards/.
22. Bolyen E, Rideout JR, Dillon MR, et al. Reproducible, interactive, scalable and extensible microbiome data science using QIIME 2. *Nat Biotechnol*. 2019;37(8):852–857.
23. Callahan BJ, McMurdie PJ, Rosen MJ, Han AW, Johnson AJA, Holmes SP. DADA2: high-resolution sample inference from Illumina amplicon data. *Nat Methods*. 2016;13(7):581–583.
24. Dobin A, Davis CA, Schlesinger F, et al. STAR: ultrafast universal RNA-seq aligner. *Bioinformatics*. 2013;29(1):15–21.
25. Chen Y, Lun ATL, Smyth GK. From reads to genes to pathways: differential expression analysis of RNA-Seq experiments using Rsubread and the edgeR quasi-likelihood pipeline. *F1000Res*. 2016;5:1438.
26. Robinson MD, McCarthy DJ, Smyth GK. edgeR: a bioconductor package for differential expression analysis of digital gene expression data. *Bioinformatics*. 2010;26(1):139–140.
27. Smyth GK. limma: linear models for microarray data. In: Gentleman R, Carey VJ, Huber W, Irizarry RA, Dudoit S, eds. *Bioinformatics and Computational Biology Solutions Using R and Bioconductor*. Statistics for Biology and Health. New York, NY: Springer; 2005:397–420, doi:10.1007/0-387-29362-0_23.
28. Sulakhe D, Balasubramanian S, Xie B, et al. Lynx: a database and knowledge extraction engine for integrative medicine. *Nucleic Acids Res*. 2014;42(Database issue):D1007–D1012.
29. Kanehisa M, Sato Y, Kawashima M, Furumichi M, Tanabe M. KEGG as a reference resource for gene and protein annotation. *Nucleic Acids Res*. 2016;44(D1):D457–D462.
30. Szklarczyk D, Gable AL, Nastou KC, et al. The STRING database in 2021: customizable protein–protein networks, and functional characterization of user-uploaded gene/measurement sets. *Nucleic Acids Res*. 2020;49(D1):D605–D612.
31. GitHub. Yang.yiluheihei/microbiomeMarker: R package for microbiome biomarker discovery. Marker 0.0.1. Published online April 13, 2020, doi:10.5281/zenodo.3749415
32. Martelli PL, Fariselli P, Casadio R. An ENSEMBLE machine learning approach for the prediction of all-alpha membrane proteins. *Bioinformatics*. 2003;19(Suppl 1):i205–i211.
33. Shin NR, Lee JC, Lee HY, et al. An increase in the Akkermansia spp. population induced by metformin treatment improves glucose homeostasis in diet-induced obese mice. *Gut*. 2014;63(5):727–735.
34. Rodriguez J, Hiel S, Delzenne NM. Metformin: old friend, new ways of action-implication of the gut microbiome? *Curr Opin Clin Nutr Metab Care*. 2018;21(4):294–301.
35. Floyd JL, Grant MB. The gut–eye axis: lessons learned from murine models. *Ophthalmol Ther*. 2020;9(3):499–513.
36. Murphy AB, Dinan TG, Cryan JF, Stanton C, Ross RP. Chapter 5 - Probiotics as curators of a healthy gut microbiota: delivering the solution. In: Hyland N, Stanton C, eds. *The Gut-Brain Axis*. San Diego, CA: Academic Press; 2016:61–88, doi:10.1016/B978-0-12-802304-4.00005-0.
37. Shivaji S. A systematic review of gut microbiome and ocular inflammatory diseases: are they associated? *Indian J Ophthalmol*. 2021;69(3):535–542.
38. Rowan S, Taylor A. Gut microbiota modify risk for dietary glycemia-induced age-related macular degeneration. *Gut Microbes*. 2018;9(5):452–457.
39. Das T, Jayasudha R, Chakravarthy S, et al. Alterations in the gut bacterial microbiome in people with type 2 diabetes mellitus and diabetic retinopathy. *Sci Rep*. 2021;11(1):2738.
40. Zysset-Burri DC, Keller I, Berger LE, et al. Retinal artery occlusion is associated with compositional and functional shifts in the gut microbiome and altered trimethylamine-N-oxide levels. *Sci Rep*. 2019;9(1):15303.
41. Zinkernagel MS, Zysset-Burri DC, Keller I, et al. Association of the intestinal microbiome with the development of neovascular age-related macular degeneration. *Sci Rep*. 2017;7(1):40826.
42. Liu A, Chang J, Lin Y, Shen Z, Bernstein PS. Long-chain and very long-chain polyunsaturated fatty acids in ocular aging and age-related macular degeneration. *J Lipid Res*. 2010;51(11):3217–3229.
43. Hou XW, Wang Y, Pan CW. Metabolomics in age-related macular degeneration: a systematic review. *Invest Ophthalmol Vis Sci*. 2020;61(14):13.
44. Bui BV, Hu RG, Acosta ML, Donaldson P, Vingrys AJ, Kalloniatis M. Glutamate metabolic pathways and retinal function. *J Neurochem*. 2009;111(2):589–599.
45. Ohashi T, Namekata K, Guo X, Kimura A, Harada C, Harada T. Effects of lighting environment on the degeneration of retinal ganglion cells in glutamate/aspartate transporter

Investigative Ophthalmology & Visual Science

deficient mice, a mouse model of normal tension glaucoma. *Biochem Biophys Rep*. 2022;29:101197.
46. Ulshafer RJ, Sherry DM, Dawson R, Wallace DR. Excitatory amino acid involvement in retinal degeneration. *Brain Res*. 1990;531(1-2):350–354.
47. Liberatore F, Bucci D, Mascio G, et al. Permissive role for mGlu1 metabotropic glutamate receptors in excitotoxic retinal degeneration. *Neuroscience*. 2017;363:142–149.
48. Agbaga MP, Mandal MNA, Anderson RE. Retinal very long-chain PUFAs: new insights from studies on ELOVL4 protein. *J Lipid Res*. 2010;51(7):1624–1642.
49. Yeboah GK, Lobanova ES, Brush RS, Agbaga MP. Very long chain fatty acid-containing lipids: a decade of novel insights from the study of ELOVL4. *J Lipid Res*. 2021;62:100030.
50. Acar İE, Lores-Motta L, Colijn JM, et al. Integrating metabolomics, genomics, and disease pathways in age-related macular degeneration: the EYE-RISK Consortium. *Ophthalmology*. 2020;127(12):1693–1709.
51. Augustin HG, Koh GY, Thurston G, Alitalo K. Control of vascular morphogenesis and homeostasis through the angiopoietin-Tie system. *Nat Rev Mol Cell Biol*. 2009;10(3):165–177.
52. Nguyen QD, Heier JS, Do DV, et al. The Tie2 signaling pathway in retinal vascular diseases: a novel therapeutic target in the eye. *Int J Retina Vitreous*. 2020;6(1):48.
53. Kim J, Park JR, Choi J, et al. Tie2 activation promotes choriocapillary regeneration for alleviating neovascular age-related macular degeneration. *Sci Adv*. 2019;5(2):eaau6732.
54. Coma S, Allard-Ratick M, Akino T, van Meeteren LA, Mammoto A, Klagsbrun M. GATA2 and Lmo2 control angiogenesis and lymphangiogenesis via direct transcriptional regulation of neuropilin-2. *Angiogenesis*. 2013;16(4):939–952.
55. De Falco S. The discovery of placenta growth factor and its biological activity. *Exp Mol Med*. 2012;44(1):1–9.
56. Chen LJ, Ma L, Chu WK, et al. Identification of PGF as a new gene for neovascular age-related macular degeneration in a Chinese population. *Invest Ophthalmol Vis Sci*. 2016;57(4):1714–1720.
57. Geerlings MJ, de Jong EK, den Hollander AI. The complement system in age-related macular degeneration: a review of rare genetic variants and implications for personalized treatment. *Mol Immunol*. 2017;84:65–76.
58. Takeda A, Baffi JZ, Kleinman ME, et al. CCR3 is a target for age-related macular degeneration diagnosis and therapy. *Nature*. 2009;460(7252):225–230.
59. Xu L, Kong L, Wang J, Ash JD. Stimulation of AMPK prevents degeneration of photoreceptors and the retinal pigment epithelium. *Proc Natl Acad Sci USA*. 2018;115(41):10475–10480.
60. Wu H, Esteve E, Tremaroli V, et al. Metformin alters the gut microbiome of individuals with treatment-naive type 2 diabetes, contributing to the therapeutic effects of the drug. *Nat Med*. 2017;23(7):850–858.
61. Forslund K, Hildebrand F, Nielsen T, et al. Disentangling type 2 diabetes and metformin treatment signatures in the human gut microbiota. *Nature*. 2015;528(7581):262–266.
62. de la Cuesta-Zuluaga J, Mueller NT, Corrales-Agudelo V, et al. Metformin is associated with higher relative abundance of mucin-degrading Akkermansia muciniphila and several short-chain fatty acid-producing microbiota in the gut. *Diabetes Care*. 2017;40(1):54–62.
63. Horai R, Zárate-Bladés CR, Dillenburg-Pilla P, et al. Microbiota-dependent activation of an autoreactive T cell receptor provokes autoimmunity in an immunologically privileged site. *Immunity*. 2015;43(2):343–353.
64. Lyzogubov V, Dasso M, Bora N, Bora PS. Role of thalidomide, senicapoc, and sodium butyrate in choroidal neovascularization. *Biochem Biophys Res Commun*. 2020;530(2):367–373.
65. Xiao X, Chen M, Xu Y, et al. Sodium butyrate inhibits neovascularization partially via TNXIP/VEGFR2 pathway. *Oxid Med Cell Longev*. 2020;2020:e6415671.
66. Maslowski KM, Vieira AT, Ng A, et al. Regulation of inflammatory responses by gut microbiota and chemoattractant receptor GPR43. *Nature*. 2009;461(7268):1282–1286.
67. Daruich A, Picard E, Boatright JH, Behar-Cohen F. Review: the bile acids urso- and tauroursodeoxycholic acid as neuroprotective therapies in retinal disease. *Mol Vis*. 2019;25:610–624.
68. Ouyang H, Mei X, Zhang T, Lu B, Ji L. Ursodeoxycholic acid ameliorates diabetic retinopathy via reducing retinal inflammation and reversing the breakdown of blood-retinal barrier. *Eur J Pharmacol*. 2018;840:20–27.
69. Maharjan P, Kim D, Jin M, et al. Preclinical evaluation of UDCA-containing oral formulation in mice for the treatment of wet age-related macular degeneration. *Pharmaceutics*. 2019;11(11):E561.
70. Woo SJ, Kim JH, Yu HG. Ursodeoxycholic acid and tauroursodeoxycholic acid suppress choroidal neovascularization in a laser-treated rat model. *J Ocul Pharmacol Ther*. 2010;26(3):223–229.
71. Espinosa-Heidmann DG, Marin-Castano ME, Pereira-Simon S, Hernandez EP, Elliot S, Cousins SW. Gender and estrogen supplementation increases severity of experimental choroidal neovascularization. *Exp Eye Res*. 2005;80(3):413–423.
72. Rubanyi GM, Johns A, Kauser K. Effect of estrogen on endothelial function and angiogenesis. *Vascul Pharmacol*. 2002;38(2):89–98.
73. Rubanyi GM, Kauser K, Johns A. Role of estrogen receptors in the vascular system. *Vascul Pharmacol*. 2002;38(2):81–88.
74. Ruddy RM, Adams KV, Morshead CM. Age- and sex-dependent effects of metformin on neural precursor cells and cognitive recovery in a model of neonatal stroke. *Sci Adv*. 2019;5(9):eaax1912.
75. Gilbert EAB, Livingston J, Garcia-Flores E, Kehtari T, Morshead CM. Metformin improves functional outcomes, activates neural precursor cells, and modulates microglia in a sex-dependent manner after spinal cord injury. *Stem Cells Translat Med*. 2023;12(6):415–428.
76. Chaudhari K, Wang J, Xu Y, et al. Determination of metformin bio-distribution by LC-MS/MS in mice treated with a clinically relevant paradigm. *PLoS One*. 2020;15(6):e0234571.
77. Silamiķele L, Silamiķelis I, Ustinova M, et al. Metformin strongly affects gut microbiome composition in high-fat diet-induced type 2 diabetes mouse model of both sexes. *Front Endocrinol (Lausanne)*. 2021;12:626359.
78. Lee H, Ko G. Effect of metformin on metabolic improvement and gut microbiota. *Appl Environ Microbiol*. 2014;80(19):5935–5943.

Investigative Ophthalmology & Visual Science